Supporting Information

# Tumor-Activated and Metal-Organic Framework Assisted Self-Assembly of Organic Photosensitizers

Yuanbo Wang, Leilei Shi, Dou Ma, Shidang Xu, Wenbo Wu, Li Xu, Majid Panahandeh-Fard, Xinyuan Zhu, Bo Wang,* and Bin Liu*

| Term | Abbreviation |
| --- | --- |
| Amine functionalized methoxy polyethylene glycol | mPEG-$NH_2$ |
| Disulfide functionalized polyethylene glycol-polymethyl methacrylate | PMMA-S-S-mPEG |
| Powder X-ray diffraction | PXRD |
| Transmission electron microscopy | TEM |
| Laser light scattering | LLS |
| Fourier transform infrared spectroscopy | FTIR |
| Thermogravimetric analyses | TGA |
| Gel-permeation chromatography | GPC |
| High-performance liquid chromatography | HPLC |
| Cetyltrimethylammonium bromide | CTAB |
| *N*-(2-(*1H*-imidazol-4-yl)ethyl)-2-bromo-2-methylpropanamide | his-BiB |
| Chlorin e6 | Ce6 |
| TdT-mediated dUTP-biotin nick end labeling | TUNEL |
| Hematoxylin and eosin | H&E |
| Analysis of variance | ANOVA |
| Inductively coupled plasma mass spectrometry | ICP-MS |

## Supplementary Experimental Section

### General Methods, Materials, and Instruments:

mPEG-$NH_2$ ($M_w$ is ~40k g/mol) was purchased from Biochempeg Scientific Inc. PMMA-S-S-mPEG ($M_w$ is ~60k g/mol) for TBD-PMMA-S-S-mPEG and Ce6-PMMA-S-S-mPEG production was purchased from Xi'an ruixi Biological Technology Co; Ltd. All the rest chemicals were purchased from Sigma-Aldrich Inc. All solvents were processed according to standard methods before use and reagents were used as purchased without purification. Milli-Q water was supplied by Milli-Q Plus System (Millipore Corporation, Bedford, USA). TBD was prepared in our previous work.[S1] $^1$H NMR spectra were recorded on 400 MHz Bruker® and $^{13}$C NMR spectra were recorded on 101 MHz Bruker®. Images of different nanoparticles (NPs) were captured under TEM (JEOL-JEM 2010F). The measurement of UV-vis absorption spectra was carried out using a UV-vis absorption spectrometer (Shimadzu, UV-1700, Japan). PL spectra were collected using a Perkin-Elmer LS-55 equipped with a xenon lamp excitation source and a Hamamatsu (Japan) 928 PMT, using 90° angle detection for solution samples. Hydrodynamic diameter and size distribution were measured by LLS with Zetasizer Nano S (Malvern Instruments Ltd, Worcestershire, UK) at room temperature. PXRD data were collected at ambient temperature on a Bruker D8 Advance diffractometer at 40 kV, 40 mA for Cu Ka (l = 1.5418 A) at a scan rate of 0.01 deg $s^{-1}$; ZIF-8 samples (around 20 mg) were placed on 1 cm × 1 cm slides for the scanning. Lifetime measurements were performed on a Horiba DeltaFlex TCSPC system equipped with NanoLED (374 nm, 240 ps) pulsed excitation sources. FTIR data were collected with a Bio-Rad FTS 3500 spectrometer under the attenuated total reflection mode. TGA was performed under air atmosphere using a Shimadzu DTG-60AH instrument. The $N_2$ and $O_2$ sorption isotherms were obtained using a Micromeritics ASAP 2020 physisorption analyzer. GPC analyses were performed *via* Waters e2695 Alliance HPLC system with Waters 2414 Refractive Index detector at a flow rate of 1.0 mL/min of HPLC grade THF as the mobile phase.

### Synthesis of ZIF-8

Nanoscale ZIF-8 without any decoration was synthesized with CTAB as a surfactant *via* a modified approach.[S2] $Zn(CH_3COO)_2$•$2H_2O$ (1.50 g, 6.8 mmol) dissolved in 25 mL of water was

added to 2-methylimidazole (5.30 g, 65 mmol) dissolved in 25 mL of 2 mM CTAB aqueous solution with gentle stirring for 1 min. The mixture turned white after 15 s and was left undisturbed at room temperature for 1 h. The product was collected by centrifugation (10000 rpm, 15 min), washed with MeOH for 3 times to offer nanoscale ZIF-8 (0.82 g, 53% yield) as white solid based on $Zn(CH_3COO)_2 \bullet 2H_2O$. The particles were kept in MeOH for further reactions without drying.

**Synthesis of ZIF-8-PMMA**

ZIF-8-PMMA was synthesized *via* a modified method.[S3] His-BiB was firstly synthesized. Histamine dihydrochloride (1 g, 13.6 mmol), triethylamine (2.54 g, 25.1 mmol, 4.6 eq) and $CHCl_3$ (100 mL) were mixed and cooled to 0 ˚C in an ice bath. The mixture was added with bromoisobutyryl bromide (0.51 g, 2.2 mmol, 2.0 eq) in dropwise. After addition, the solution was stirred under room temperature overnight. The reaction was quenched using 100 mL of 10% KOH aqueous solution. After quenching, the solution was extracted with $CH_2Cl_2$. The organic layer was collected and dried over $MgSO_4$. After removing $CH_2Cl_2$, the crude product was recrystallized with EtOAc under -80 ˚C to give his-BiB (0.9 g, 63 % yield) as dark yellow solid. $^1$H NMR (400 MHz, $CD_3OD$): $\delta$ 7.58 (s, 1H), 6.86 (s, 1H), 3.44 (t, J = 7.2 Hz, 2H), 2.80 (t, J = 7.2 Hz, 2H), 1.88 (s, 6H).

After his-BiB synthesis, ZIF-8 (0.56 g, 4.9 mmol) was dispersed in 40 mL of 1-BuOH to exchange solvent from MeOH to 1-BuOH by centrifugation (10000 rpm, 20 min). The ZIF-8 solution and the his-BiB mixture (2.55 g, 9.8 mmol, 1.0 eq) were mixed together and the resulting suspension was sonicated for 30 min before stirred at 120 °C for 6 h. After cooling to room temperature, the particles were collected by centrifugation (10000 rpm, 20 min). After washing with MeOH, the ZIF-8 particles were soaked in MeOH for 24 h to remove 1-BuOH *via* solvent exchange. (450 mg, 80% yield). The resulting ligand-exchanged ZIF-8 (100 mg) was mixed with 5 mL of methanol, followed by ultrasonic treatment for 60 min. Then, the ligand-exchanged ZIF-8 particles were added with methyl methacrylate without polymerization inhibitor (1 g, 10.5 mmol), 0.5 mL of $CuCl_2$-PMDETA (*N, N, N', N'', N'''*-pentamethyldiethylenetriamine) stock solution (containing 0.0023 mmol $CuCl_2$, 0.023 mmol PMDETA) under magnetic stirring. After that, the vial was sealed after degassed by argon. After 30 min, a degassed solution of ascorbic acid (17 mg, 0.1 mmol) in 1 mL of MeOH was added *via* a syringe. The reaction was kept at room temperature for 10 h. The particles were collected by centrifugation (10000 rpm, 5 min) and washed with MeOH

and toluene for 3 times, respectively. The yielded ZIF-8-PMMA (130 mg) was stored in MeOH for further analyses and modifications. After DCl digestion, the precipitate (14800 rpm, 5 min) was characterized *via* $^1$H NMR (400 MHz, $CDCl_3$) (Figure S2).

**Preparations of TBD-PMMA-S-S-mPEG and Ce6-PMMA-S-S-mPEG**

The THF mixture containing TBD or Ce6 (1 mg) and purchased PMMA-S-S-mPEG (4 mg) was poured into water with 10-fold dilution. The THF/water mixture was then sonicated for 1 min using a microtip ultrasound sonicator at 12 W output (XL2000, Misonix Incorporated, NY). After THF evaporation by stirring the obtained suspension in a fume hood overnight, the obtained TBD-PMMA-S-S-mPEG and Ce6-PMMA-S-S-mPEG (0.11 mg/mL based on TBD or Ce6) were subjected to filtration through a 0.2 μm syringe driven filter and collected for further study.

**Cell Culture**

Cancerous 4T1 cells were purchased from Perkin Elmer Inc. and maintained in our lab. The 4T1 were cultured on Thermo Scientific cell culture flasks in RMPI-1640 medium (with 10% FBS, 1% penicillin/streptomycin). The cells were maintained in an atmosphere of 5% $CO_2$ and 95% humidified air at 37 °C.

**Tumor Mouse Model**

Experiment protocols involving animals were authorized by the Animal Ethics Committee of Shanghai Jiao Tong University School of Medicine (Approved number: A2018057). Mouse-based fluorescence imaging was conducted in accordance with guidelines approved by the ethics committee of Beijing Institute of Technology. The xenograft tumor model was generated by subcutaneous injection of 4T1 cancer cells ($1\times10^6$) suspended in 30 μL of saline into the right shoulder of the mouse. BALB/c mice bearing 4T1 tumors were randomly divided into 5 groups when the tumors grew to 300-400 $mm^3$.

***In Vivo* Mouse-Based Fluorescence Imaging**

Different TBD agents (injection volume = 100 μL, [TBD] = 0.5 mg $mL^{-1}$) were injected into 4T1 tumor-bearing mice through the tail vein. *In vivo* fluorescence imaging was performed at different time points post injection using an IVIS Lumina XRMS *In-vivo* Imaging System (PerkinElmer Inc, Waltham, Massachusetts, USA). The mice were anesthetized with isoflurane and imaged at the indicated time points. The excitation wavelength was set at 450 nm, and the emission

wavelength was chosen from 630 to 680 nm. At 1-day and 7-day post injection, the mice were sacrificed. The tumor and normal tissues (heart, lung, kidney, spleen, liver, and skin) were excised and washed with PBS (1×) for the *ex vivo* fluorescence imaging.

**Histological Studies**

In the histological assay, the paraffin-embedded tumor samples were cut into 5 μm thick sections, then dewaxed and rehydrated. After quenching endogenous peroxidase, achieving antigen retrieval and blocking non-specific binding sites, incubation with primary antibodies was carried out overnight at 4 °C. The antibodies used here were monoclonal anti-CD31 antibodies (1:200) (Beijing Biosynthesis Biotechnology Co., LTD). Biotinylated goat anti-rabbit antibodies were used as secondary antibodies at 1:200 for 30 min at room temperature. The samples were stained with H&E for microscopic observation. Apoptosis of the tumor cells was determined by the TUNEL method according to the manufacturer's instructions.

**Statistical Analysis**

Quantitative data were expressed as mean ± standard deviation. ANOVA analysis and Student's T-test were performed in Excel and utilized for statistical contrast. $P < 0.05$ was figured statistically significant.

## Supplementary Experimental Section

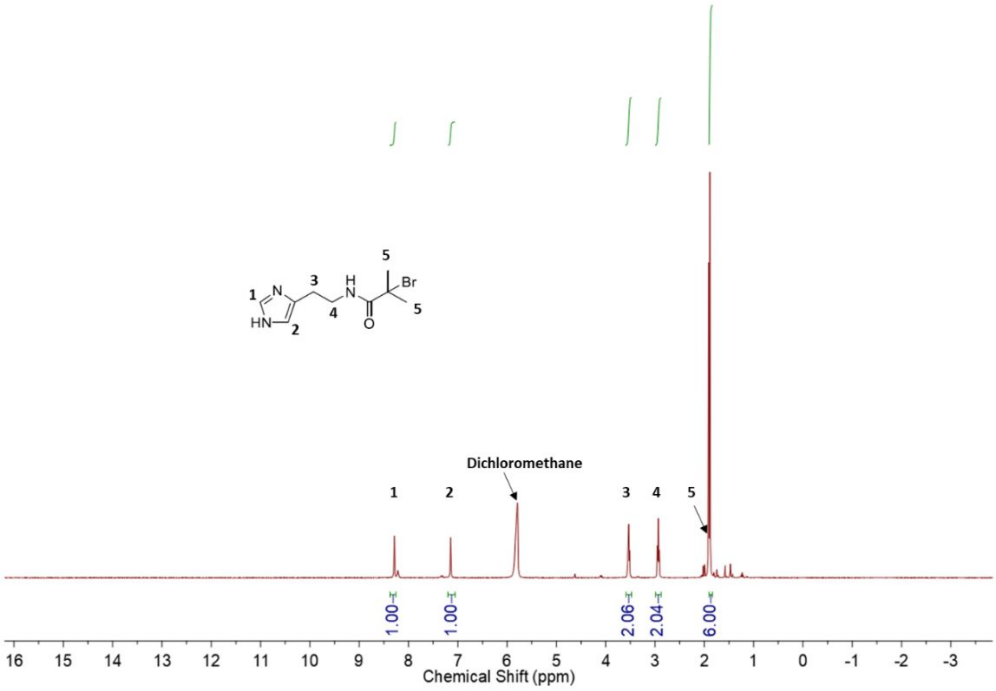


**Figure S1.** NMR spectrum of his-BiB in $CD_3OD$.

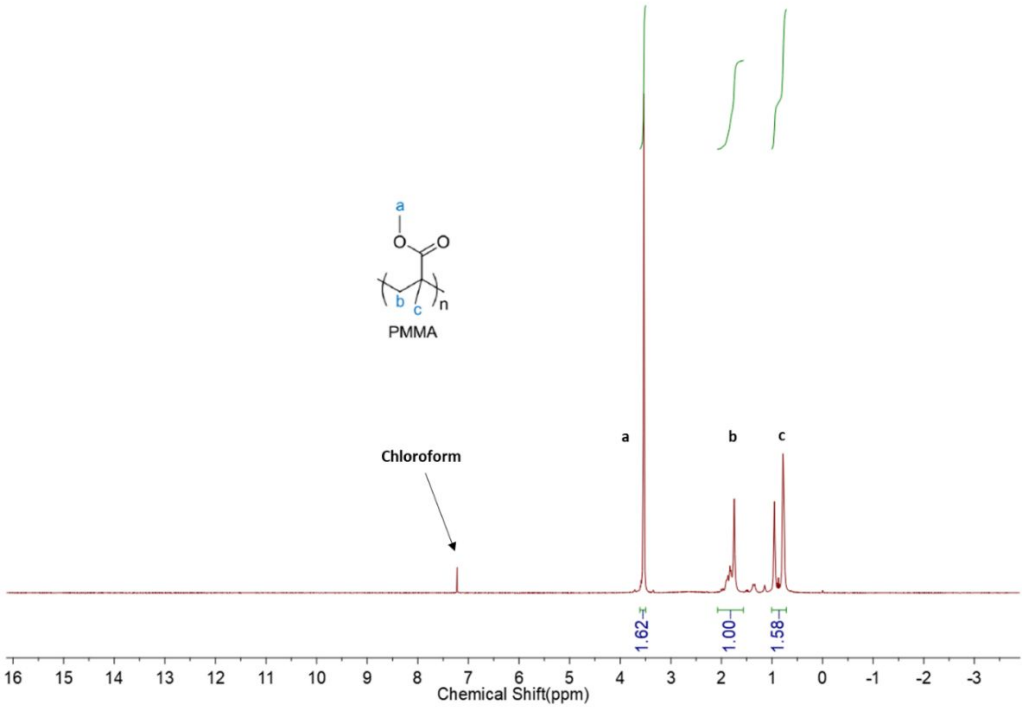


**Figure S2.** NMR spectrum of digested ZIF-8-PMMA in $CDCl_3$.

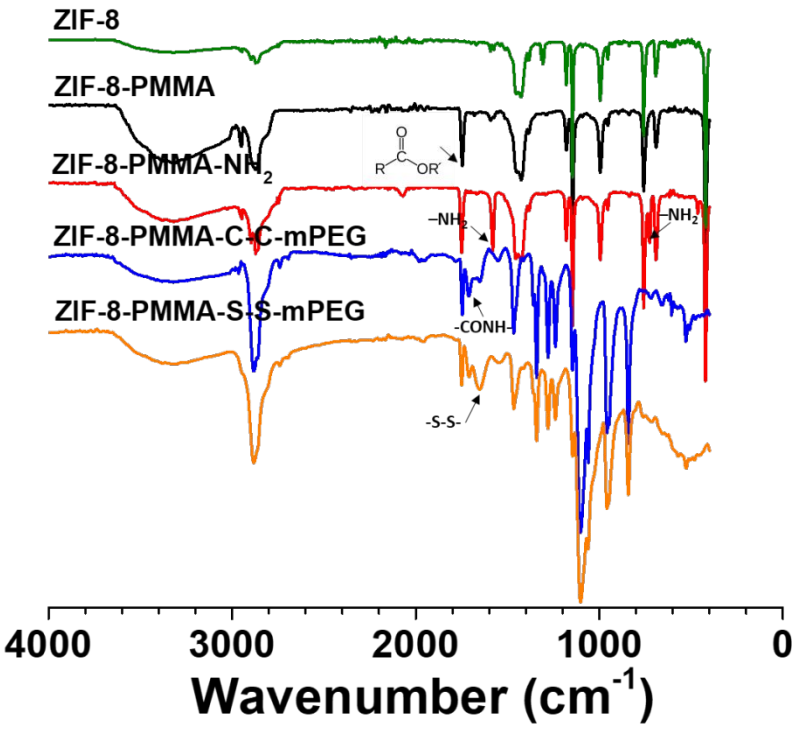


**Figure S3.** FT-IR spectra of ZIF-8-PMMA, ZIF-8-PMMA-$NH_2$, ZIF-8-PMMA-C-C-mPEG, and ZIF-8-PMMA-S-S-mPEG.

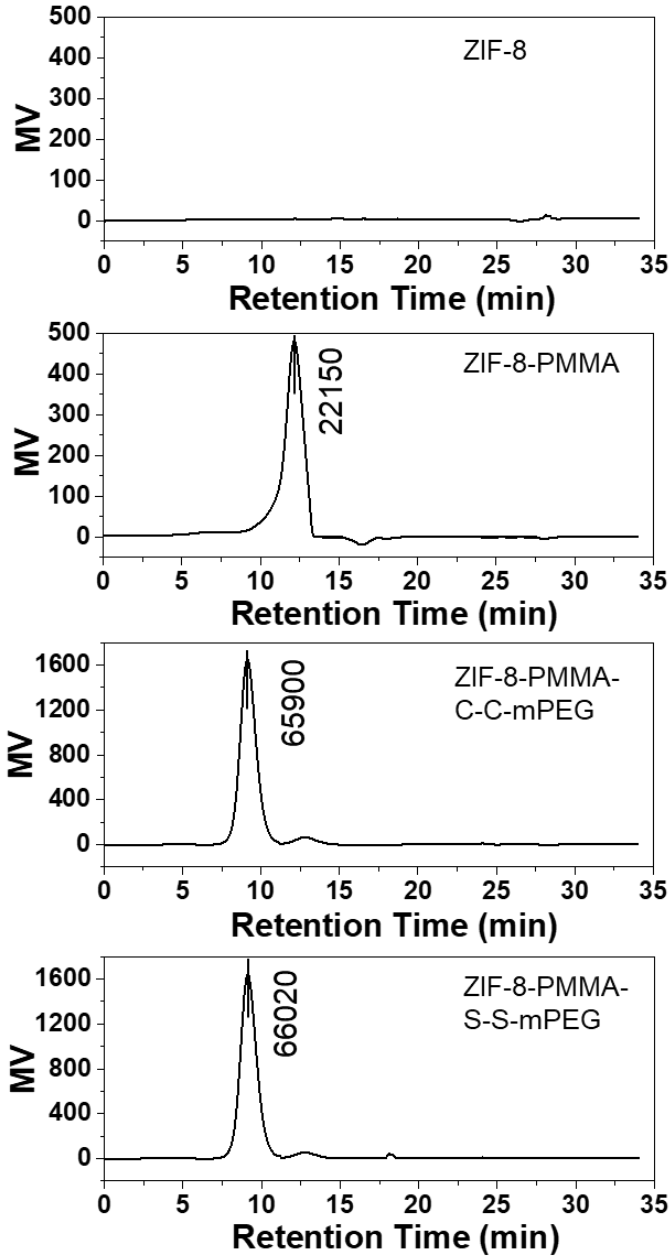


**Figure S4.** GPC results of hydrochloric acid digested ZIF-8-PMMA, ZIF-8-PMMA-C-C-mPEG, and ZIF-8-PMMA-C-C-mPEG (10 mg $mL^{-1}$) treated with GSH (1 mM, 2 h).

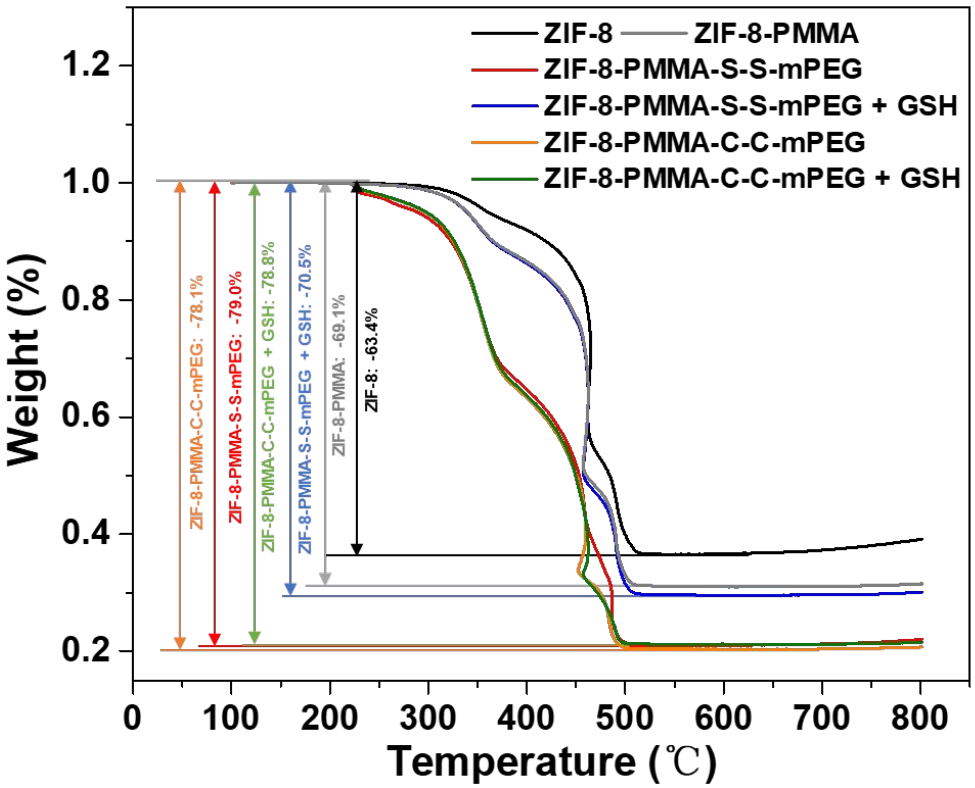


**Figure S5.** TGA data for ZIF-8, ZIF-8-PMMA, ZIF-8-PMMA-S-S-mEPG, and ZIF-8-PMMA-C-C-mEPG before or after GSH treatment. The samples after GSH treatment are collected by centrifugation before TGA analysis.

| Material | Weight loss (%) | ZIF-8 wt content (%) | BET surface area ($m^2/g$) | $O_2$ adsorbed volume at 1 atm and RT ($cm^3_{stp}/g$) |
|---|---|---|---|---|
| **ZIF-8** | 63.4 | 100 | 1605±30 | 1.3±0.1 |
| **ZIF-8-PMMA** | 69.1 | 91 | 1346±61 | 1.1±0.2 |
| **ZIF-8-PMMA-S-S-mPEG** | 79.0 | 73 | 1288±77 | 1.1±0.2 |
| **ZIF-8-PMMA-S-S-mPEG + GSH** | 70.5 | 89 | 1335±80 | 0.9±0.3 |
| **ZIF-8-PMMA-C-C-mPEG** | 78.1 | 74 | 1302±65 | 1.1±0.2 |
| **ZIF-8-PMMA-C-C-mPEG + GSH** | 78.8 | 73 | 1293±89 | 1.0±0.2 |

**Table S1.** Summary of weight loss of TGA measurements, ZIF-8 loading calculated form the weight loss, BET Surface Area, and $O_2$ adsorbed volume of different MOF particles.

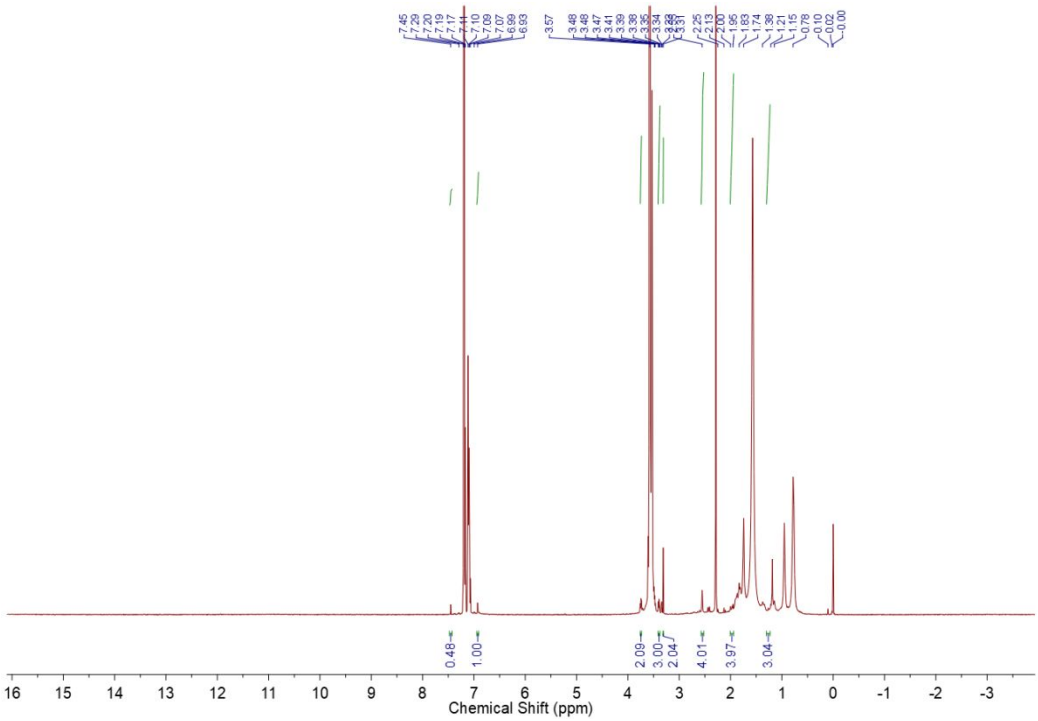


**Figure S6.** [1]H NMR spectrum of digested ZIF-8-PMMA-S-S-mPEG in MeOD.

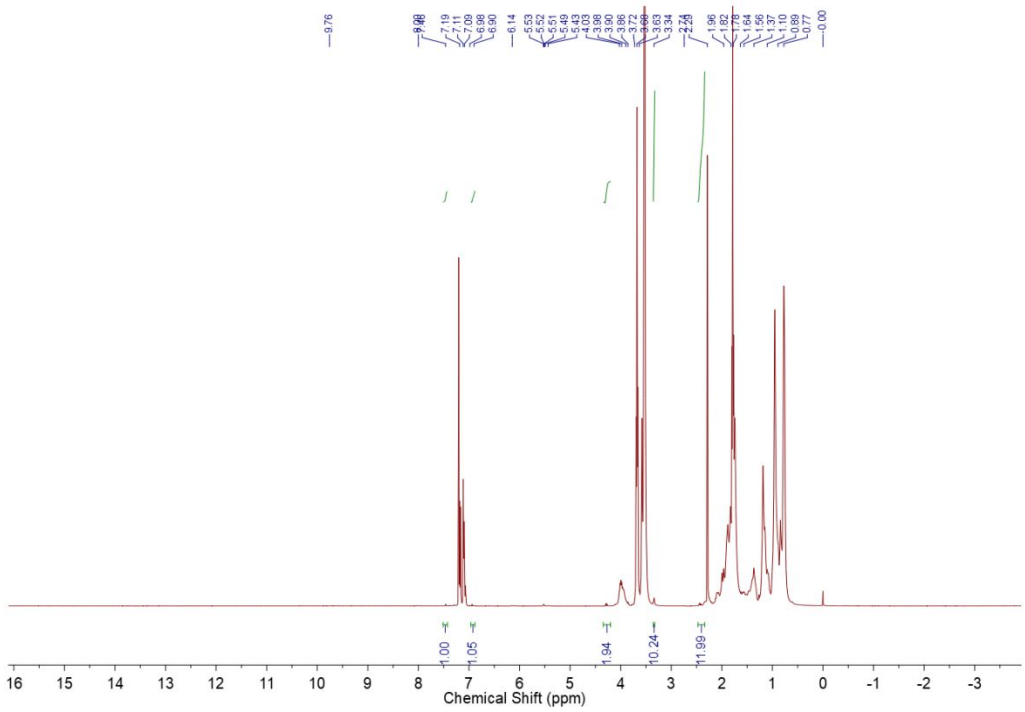


**Figure S7.** [1]H NMR spectrum of digested ZIF-8-PMMA-C-C-mPEG in MeOD.

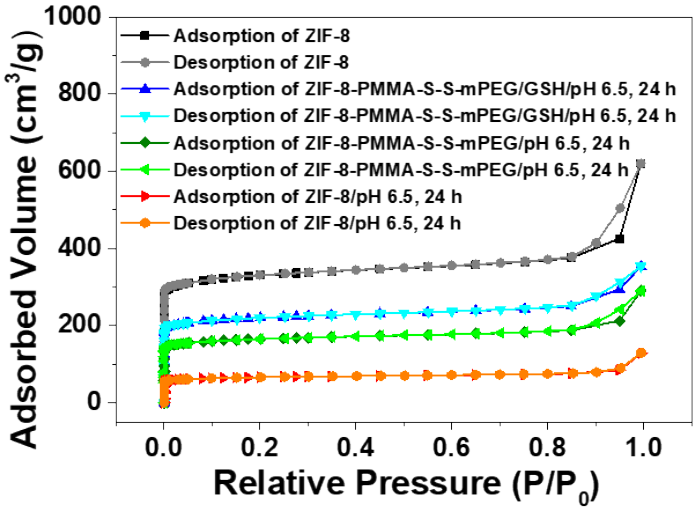


**Figure S8.** $N_2$ adsorption and desorption isotherms of ZIF-8-PMMA-S-S-mPEG before or after GSH treatment (1 mM, PBS, 1×, at pH 6.5, 2 h) and ZIF-8 with or without immersion in PBS (1×) at pH 6.5 (24 h) at 77 K.

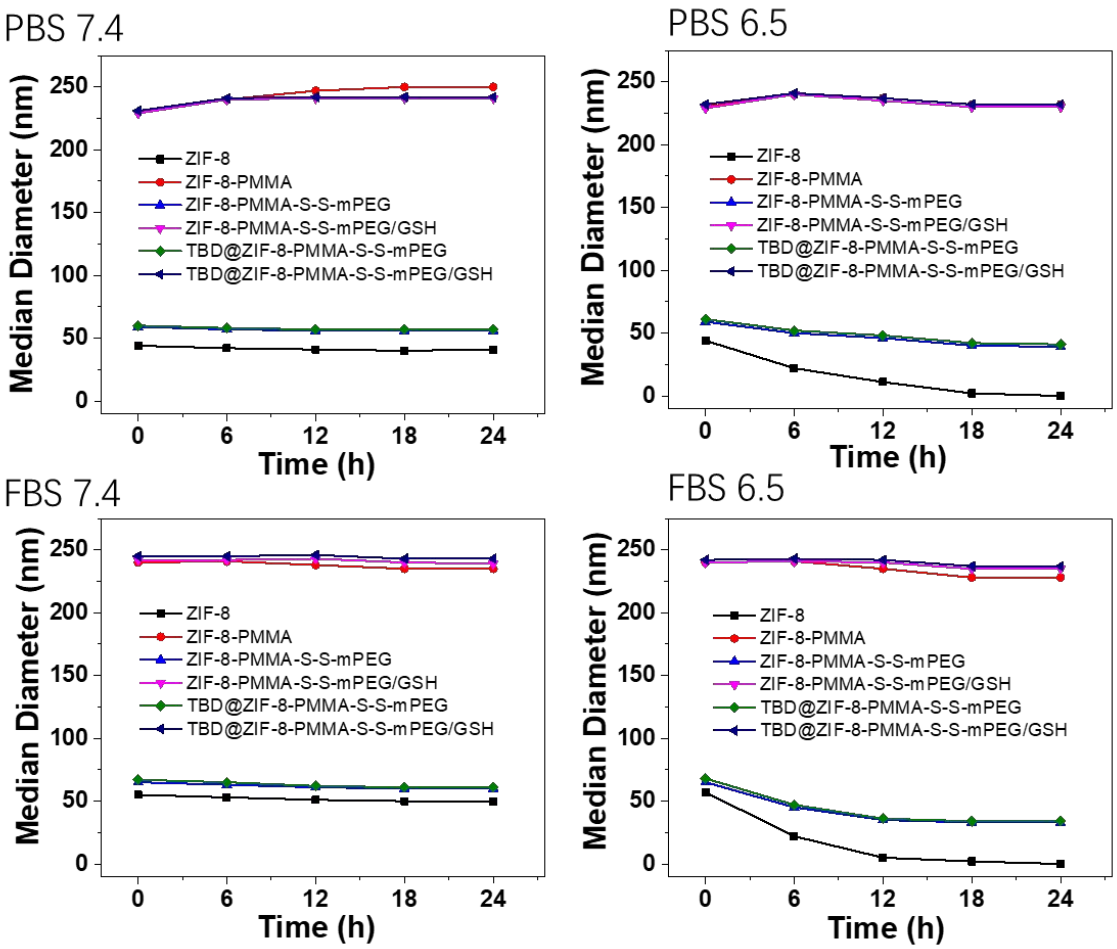


**Figure S9.** Median diameters of different ZIF-8 agents immersed in PBS (1×) or FBS at pH 7.4 or 6.5 for different time.

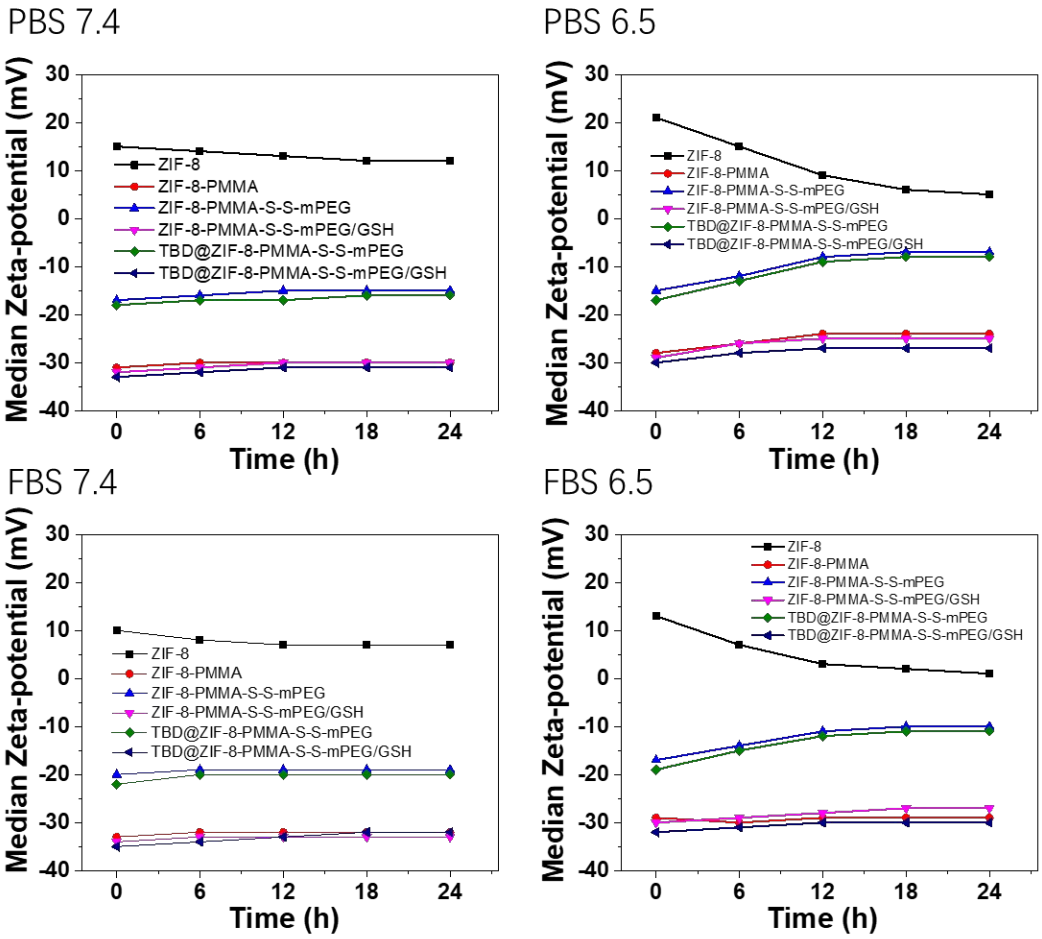


**Figure S10.** Median zeta-potentials of different ZIF-8 agents immersed in PBS (1×) or FBS at pH 7.4 or 6.5 for different time.

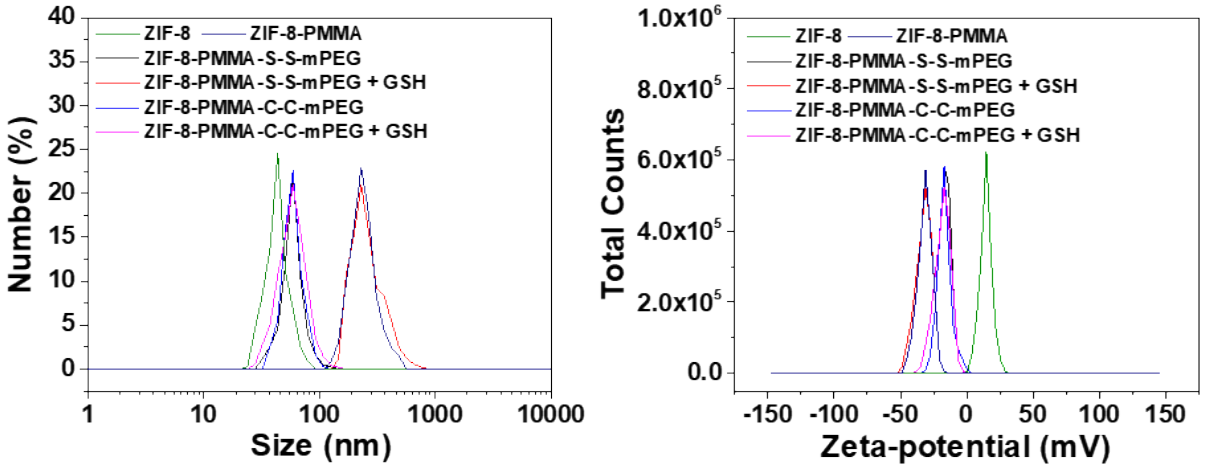


**Figure S11.** DLS results and zeta-potentials of ZIF-8, ZIF-8-PMMA, ZIF-8-PMMA-S-S-mPEG, and ZIF-8-PMMA-C-C-mPEG (10 μg $mL^{-1}$) before or after GSH treatment (1 μM, 2 h).

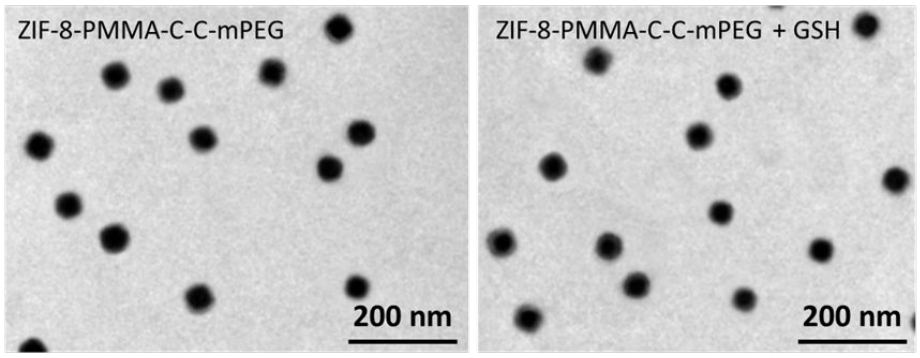


**Figure S12.** Representative TEM images of ZIF-8-PMMA-C-C-mPEG (10 μg $mL^{-1}$) before and after GSH treatment (1 μM, 2 h).

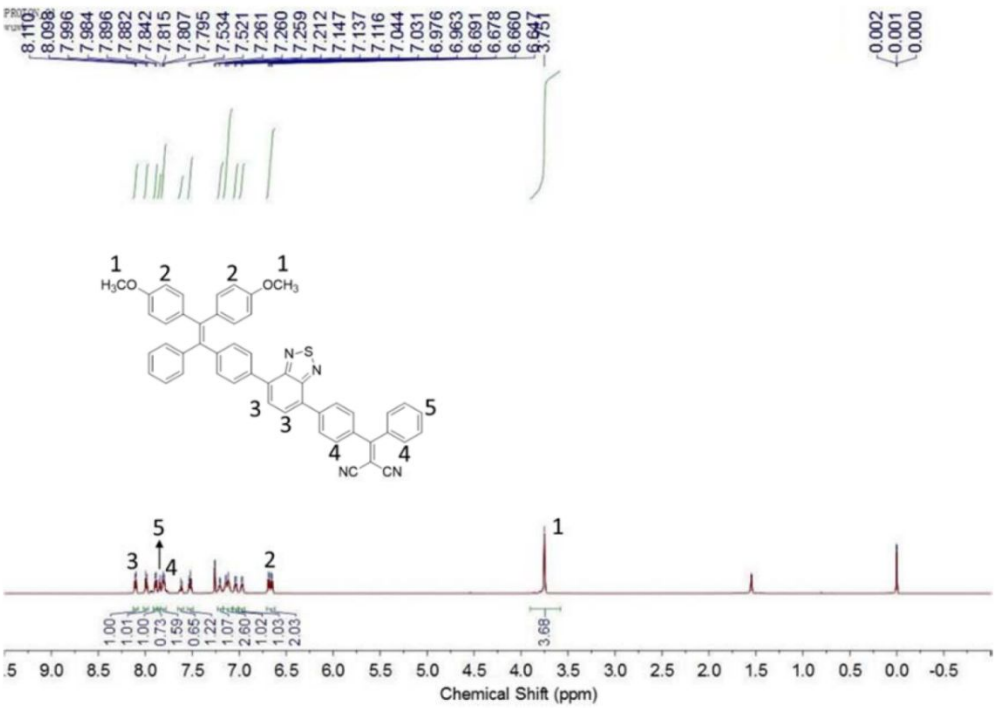


**Figure S13.** $^{1}$H NMR spectrum of TBD in chloroform-*d*.

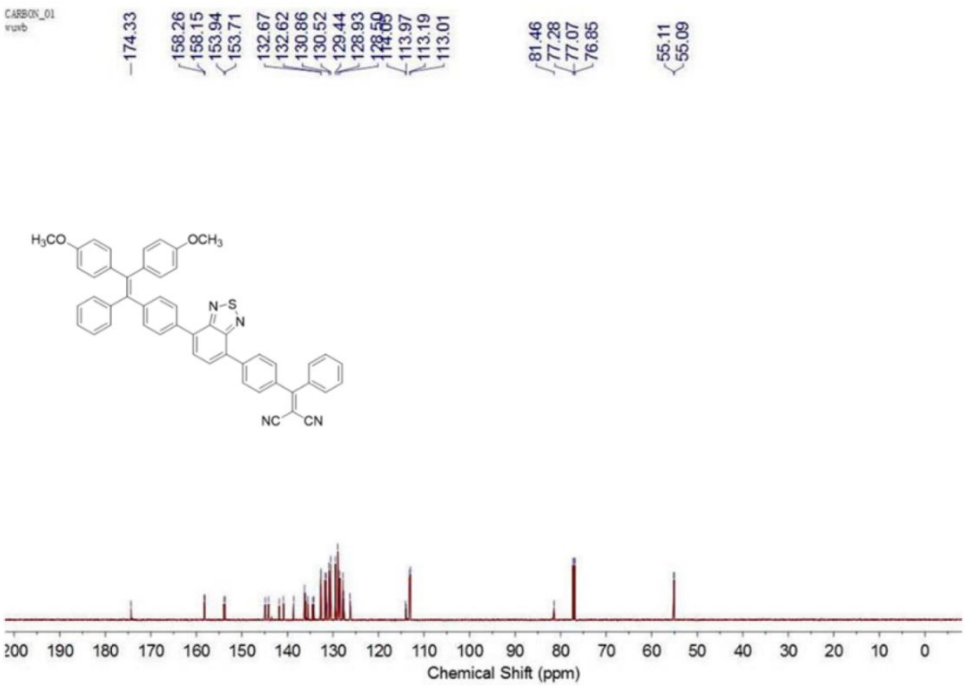


**Figure S14.** $^{13}$C NMR spectrum of TBD in chloroform-*d*.

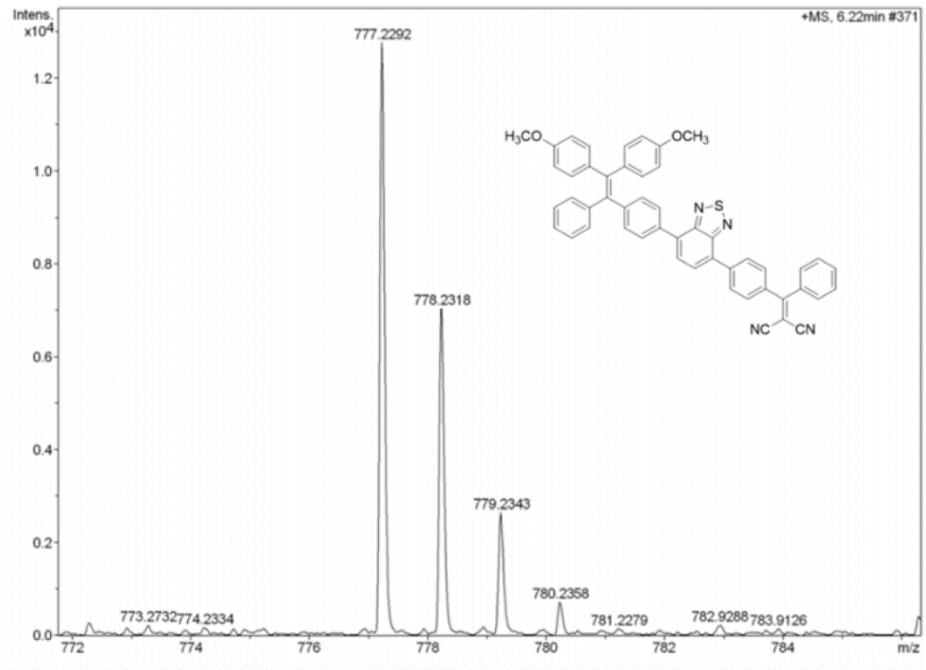


**Figure S15.** High-resolution mass spectrum of TBD. The peak of 777.2292 is the molecular ion peaks ($[M+Na]^+$), while the other peaks are the isotopic ion peak.

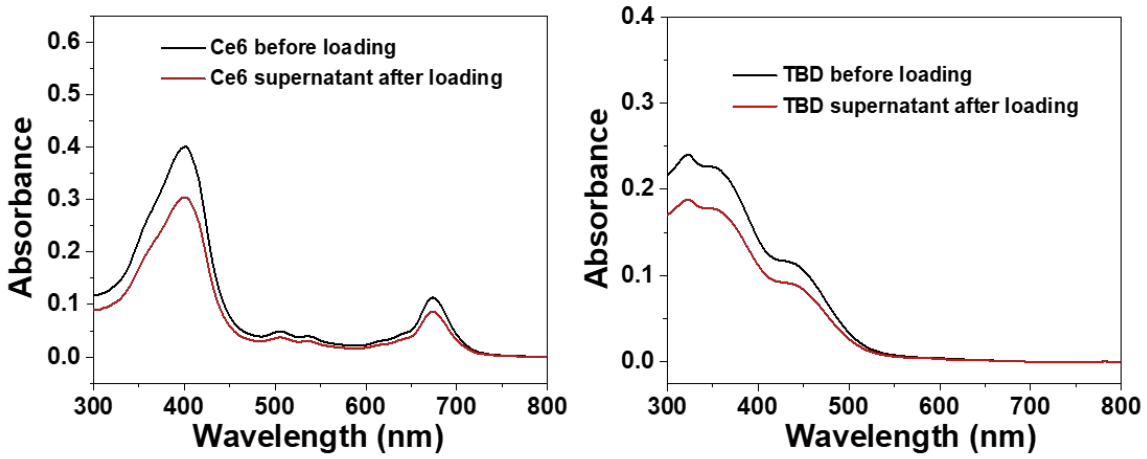


**Figure S16.** UV-vis absorption spectra of Ce6 and TBD before and after encapsulated into ZIF-8 during its synthesis. For measurement, [Ce6] = [TBD] = 1 μg $mL^{-1}$. For loading process, [Ce6] = [TBD] = 2 mg $mL^{-1}$.

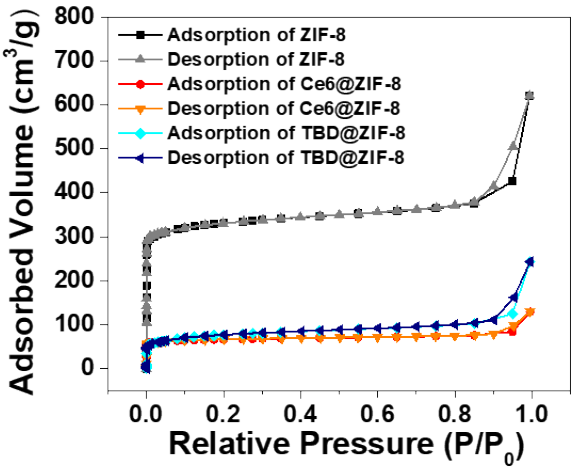


**Figure S17.** $N_2$ adsorption and desorption isotherms of ZIF-8, Ce6@ZIF-8, and TBD@ZIF-8 at 77 K.

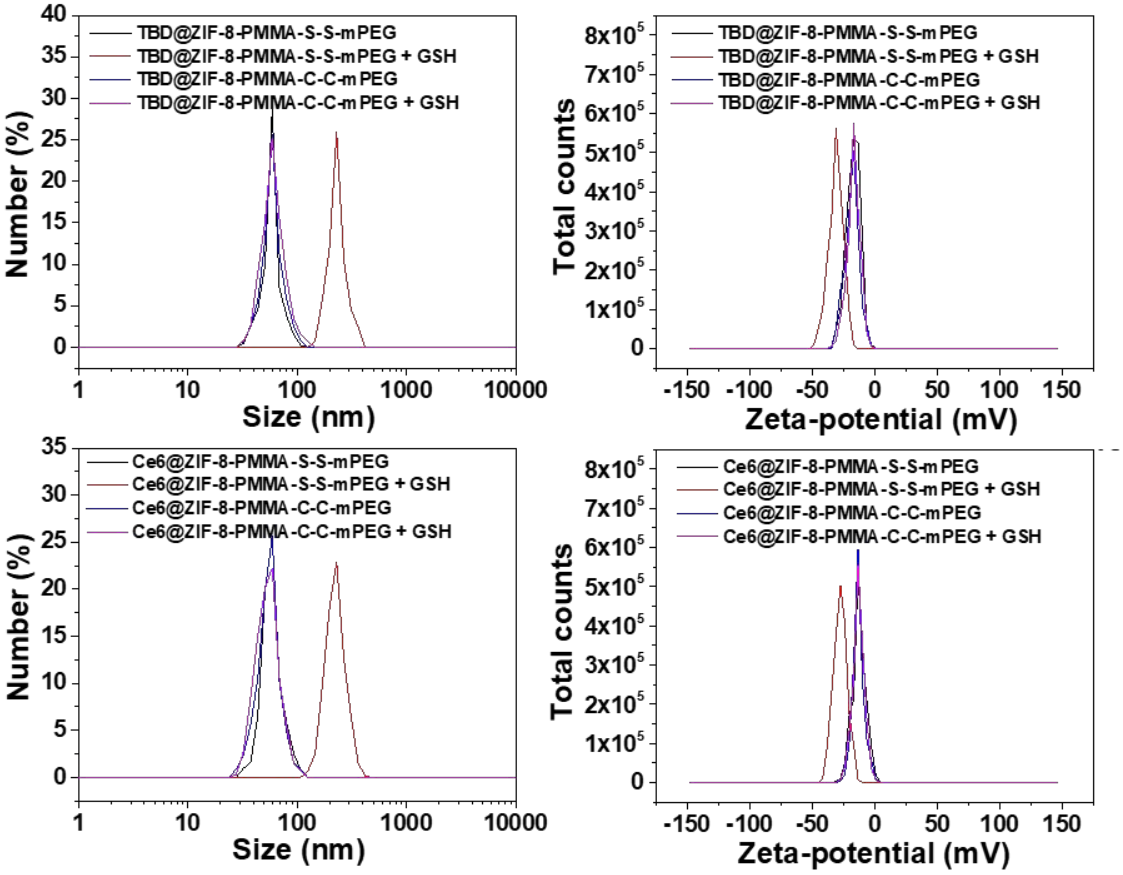


**Figure S18.** DLS results and zeta-potentials of TBD@ZIF-8-PMMA-S-S-mPEG, TBD@ZIF-8-PMMA-C-C-mPEG, Ce6@ZIF-8-PMMA-S-S-mPEG, and Ce6@ZIF-8-PMMA-C-C-mPEG (2.5 μg $mL^{-1}$ based on TBD or Ce6) before or after GSH treatment (1 μM, 2 h).

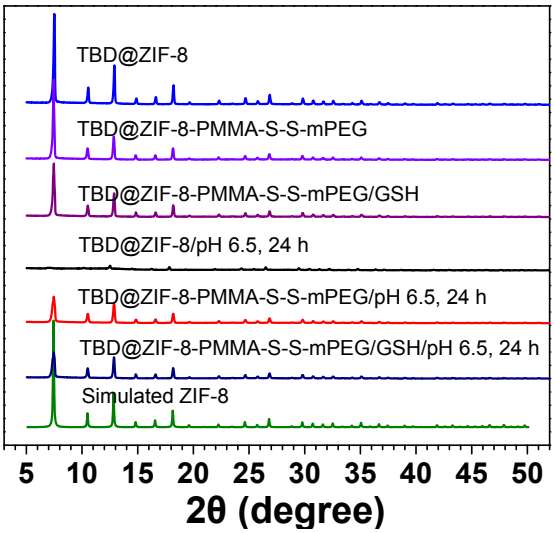


**Figure S19.** PXRD patterns of TBD@ZIF-8-PMMA-S-S-mPEG (10 mg $mL^{-1}$) before or after GSH treatment (1 mM, PBS, 1×, at pH 6.5, 2 h) and TBD@ZIF-8 with or without immersion in PBS (1×) at pH 6.5 (24 h).

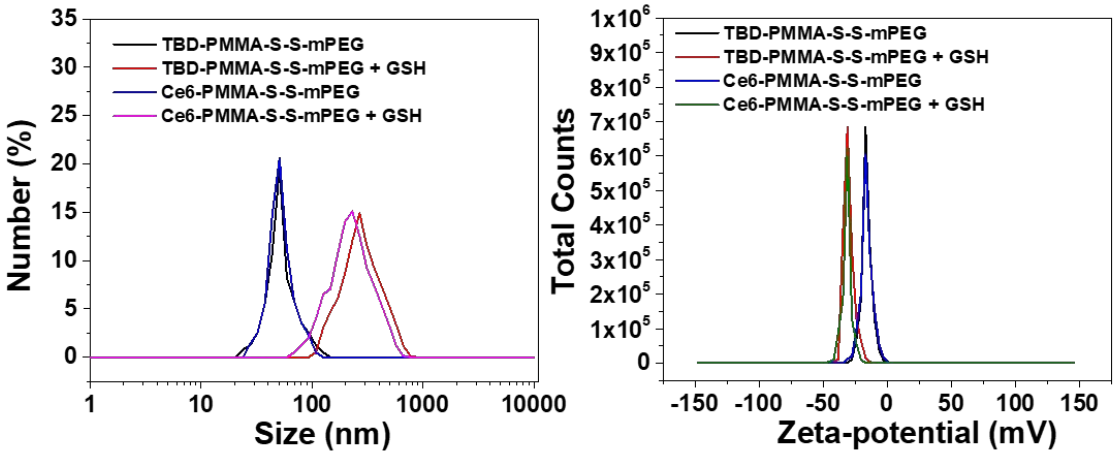


**Figure S20.** DLS results and zeta-potentials of TBD-PMMA-S-S-mPEG and Ce6-PMMA-S-S-mPEG (2.5 μg $mL^{-1}$ based on TBD or Ce6) before or after GSH treatment (1 μM, 2 h).

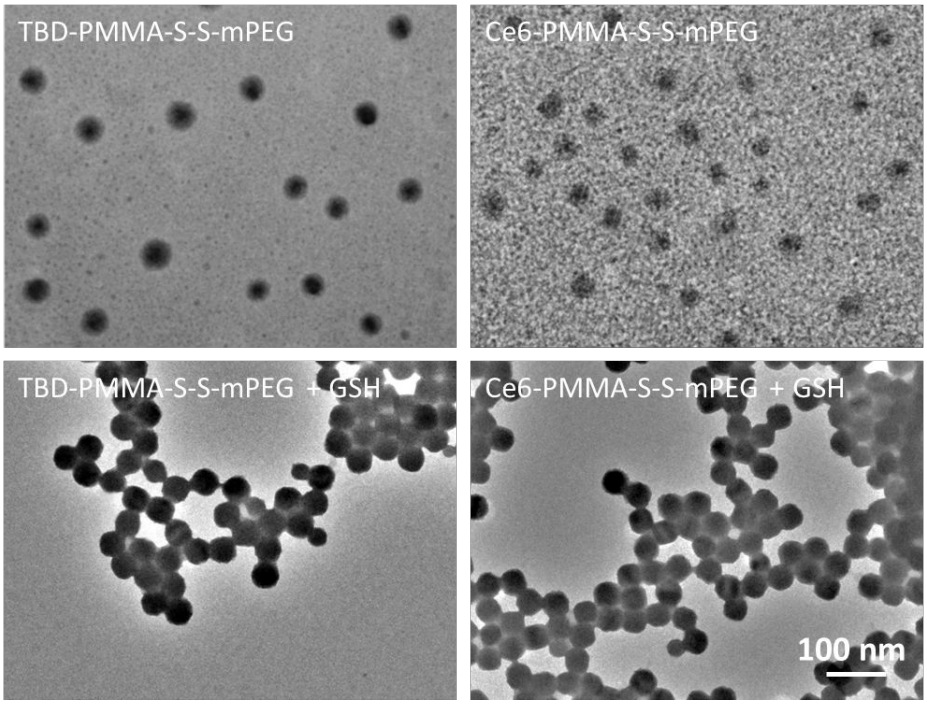


**Figure S21.** TEM images of TBD-PMMA-S-S-mPEG and Ce6-PMMA-S-S-mPEG (2.5 μg $mL^{-1}$ based on TBD or Ce6) before or after GSH treatment (1 μM, 2 h).

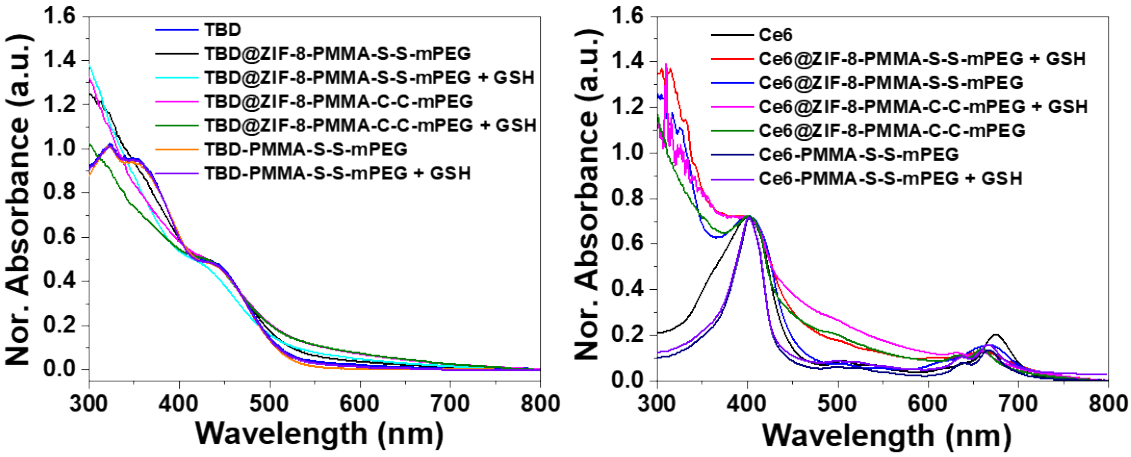


**Figure S22.** Normalized absorption spectra of TBD- and Ce6-incorporated agents before or after GSH treatment.

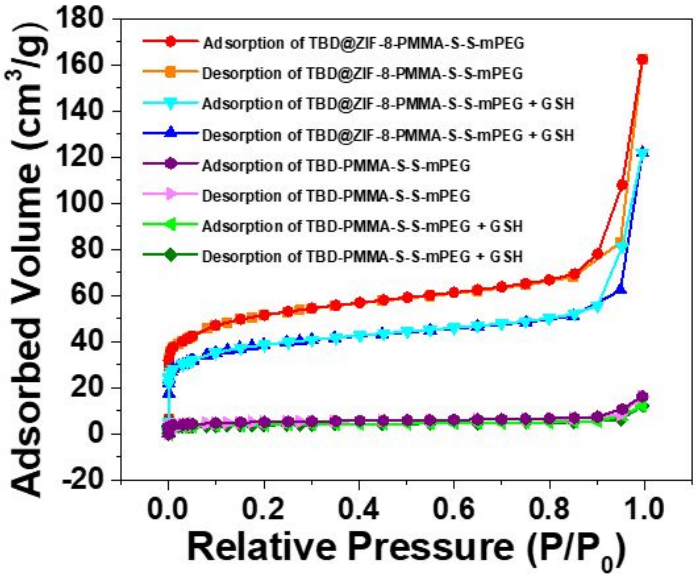


**Figure S23.** $N_2$ adsorption and desorption isotherms of TBD-PMMA-S-S-mPEG and TBD@ZIF-8-PMMA-S-S-mPEG before or after GSH treatment at 77 K.

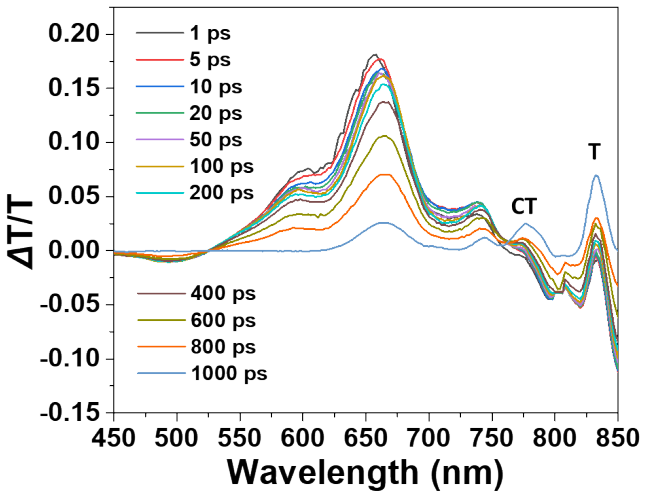


**Figure S24.** Transient absorption spectra of TBD@ZIF-8-PMMA-S-S-mPEG (50 μg $mL^{-1}$) treated by GSH (20 μM, 2h) at indicated delay time following photoexcitation at 450 nm. CT is short for charge transfer, and T is short for triplet.

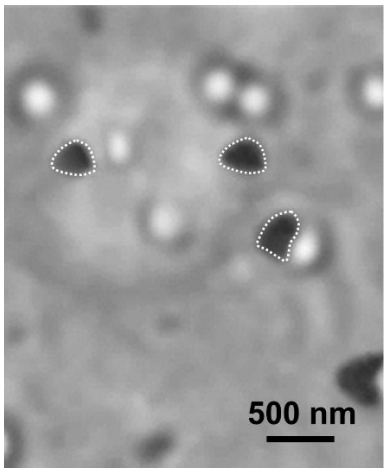


**Figure S25.** Enlarged image of 4T1 treated by TBD@ZIF-8-PMMA-S-S-mPEG under bright field. Triangular assemblies indicated by yellow arrows in Figure 3A were circled by white dot-line for better visualization.

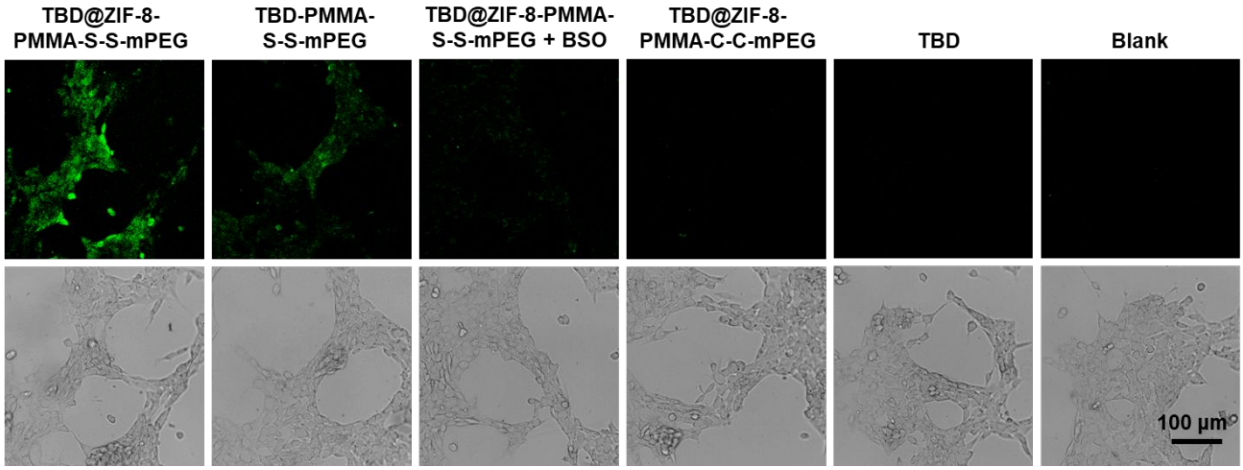


**Figure S26.** CLSM images of 4T1 cells upon incubation with different PS agents (10 μg $mL^{-1}$), ROS Detection Kit, and further treatment with white light. Illumination intensity, time, and wavelength are 60 mW $cm^{-2}$, 5 min, and 400-700 nm, respectively.

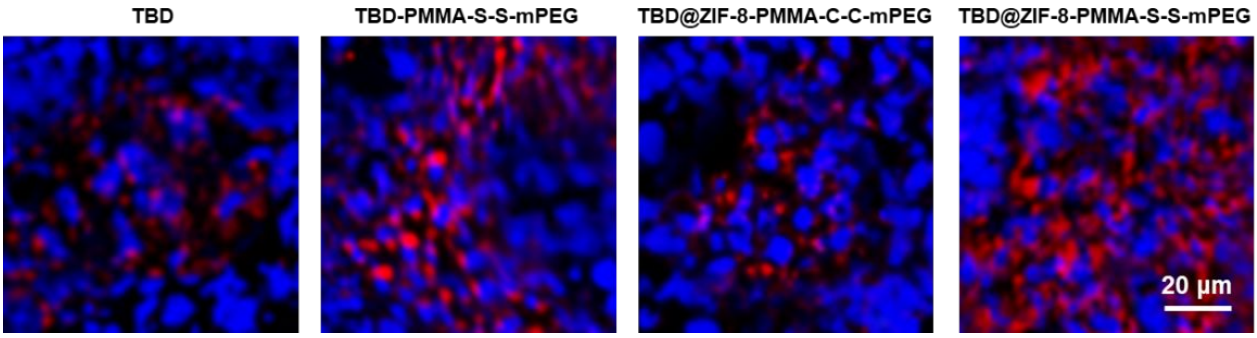


**Figure S27.** Enlarged tumor regions circled by white dot-line in Figure 4D to show different morphologies of different agents localized inside tumor. All the images share the same scale bar.

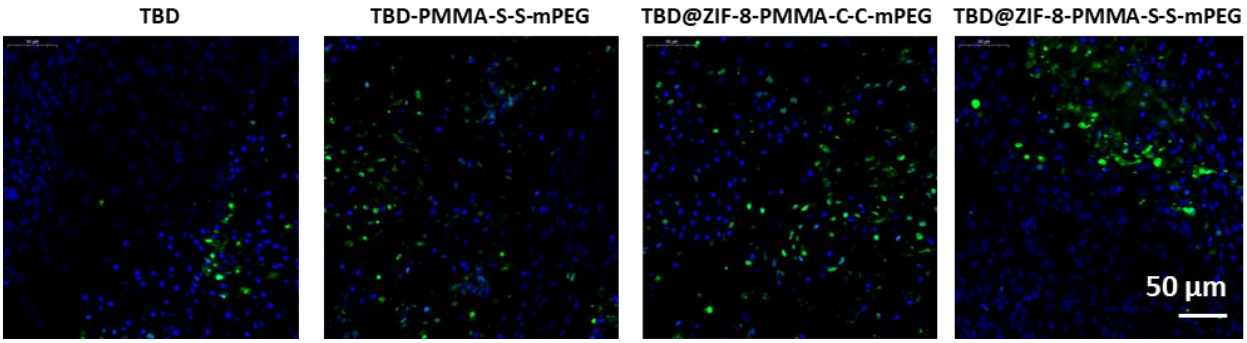


**Figure S28.** TUNEL immunostaining performed on skin slices of 4T1 tumor-bearing mice. The normal skin was subcutaneously injected with different agents and treated with white light before sectioned. Injection volume = 100 μL, [TBD] = 0.5 mg $mL^{-1}$. Illumination intensity, time, and wavelength are 300 mW $cm^{-2}$, 10 min, and 400-700 nm, respectively.

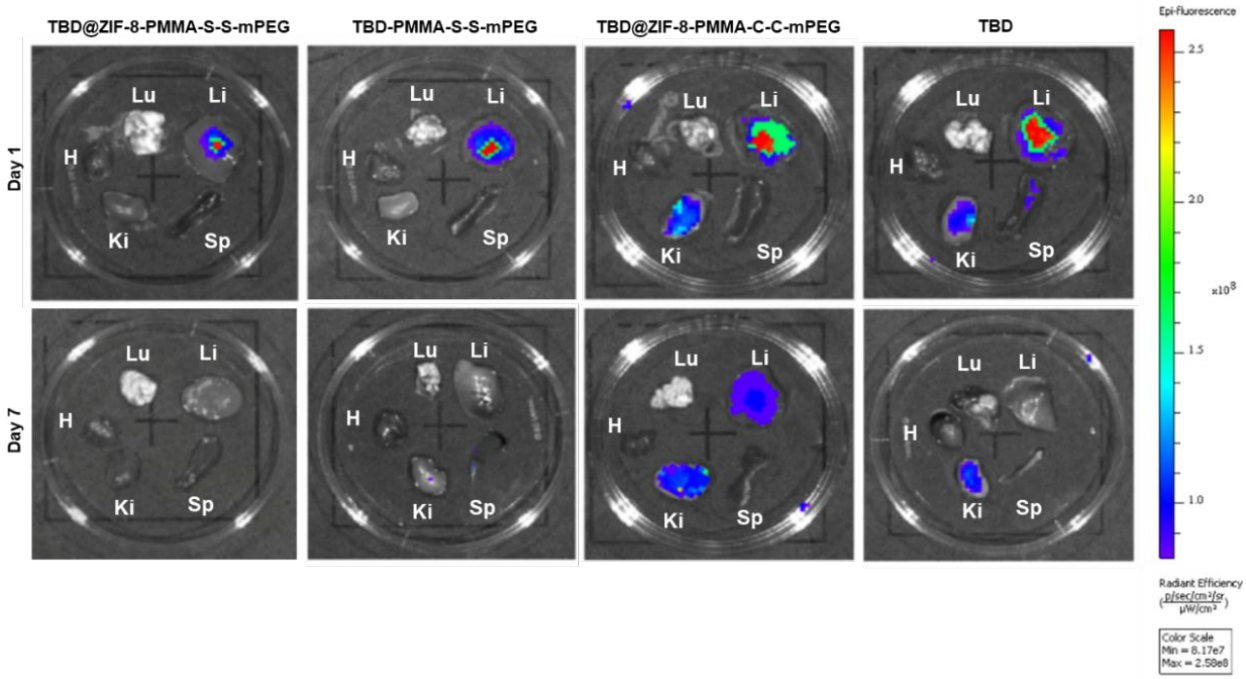


**Figure S29.** Fluorescence images and intensities of the internal organs after anatomy for different treatment (intravenous injection) at Day 1 and Day 7. The color bar corresponds to the detected fluorescence intensity.

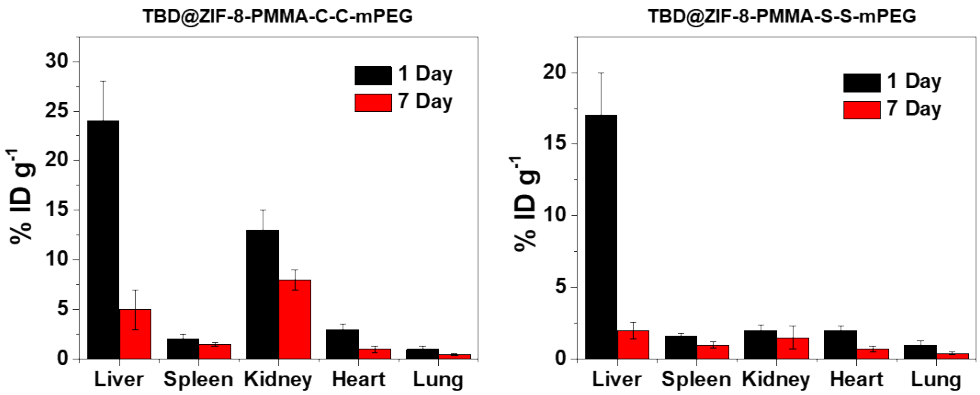


**Figure S30.** Biodistribution of different agents on Day 1 and Day 7 after intravenous administration based on ICP-MS analysis (data expressed as percent injected dose per gram of tissue (% ID/g tissue), $n = 3$ mice per group.

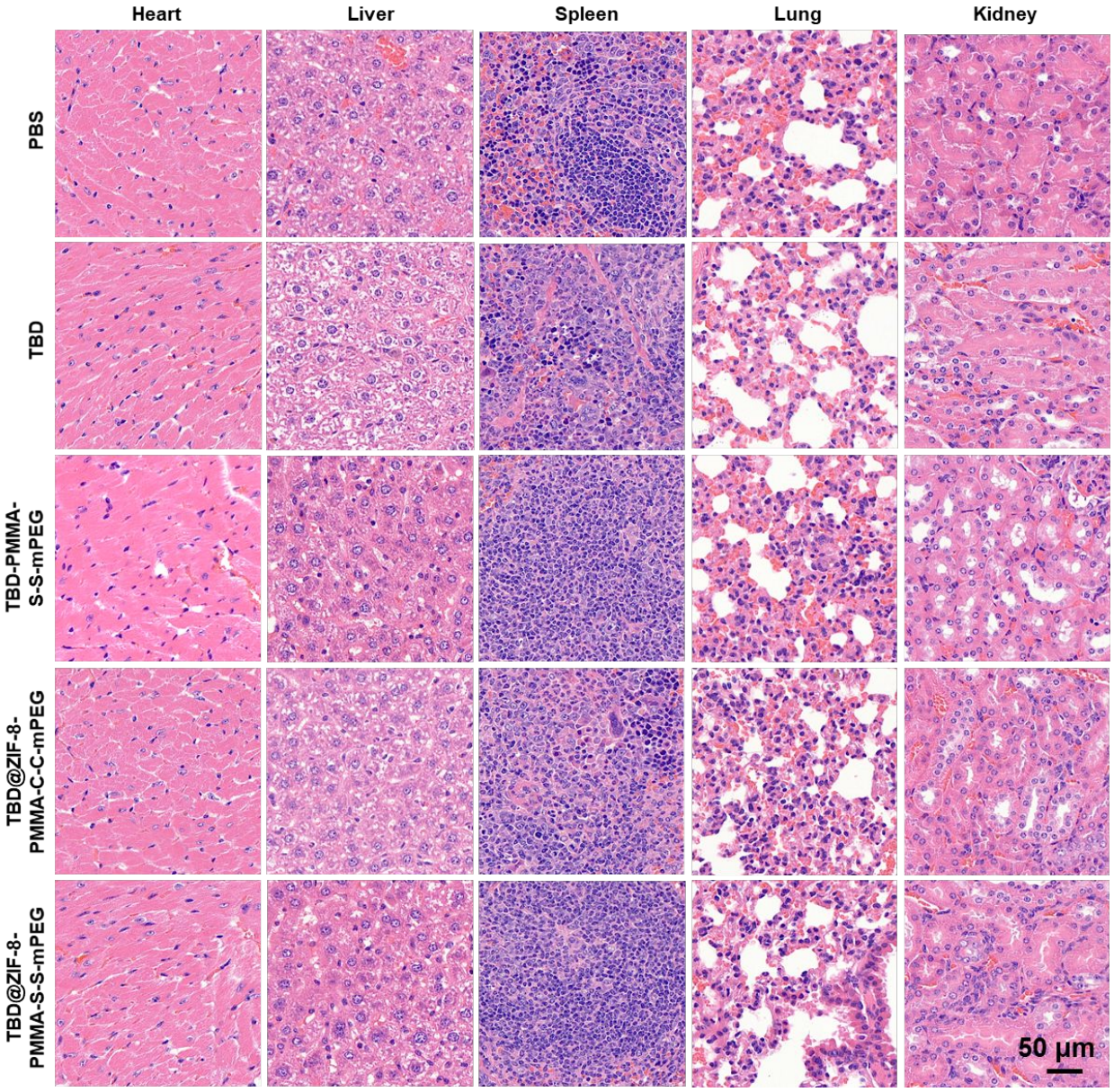


**Figure S31.** Typical images of H&E-stained heart, liver, spleen, lung, and kidney slices from mice after intravenous administration of different agents after 7 days. All the images share the same scale bar.

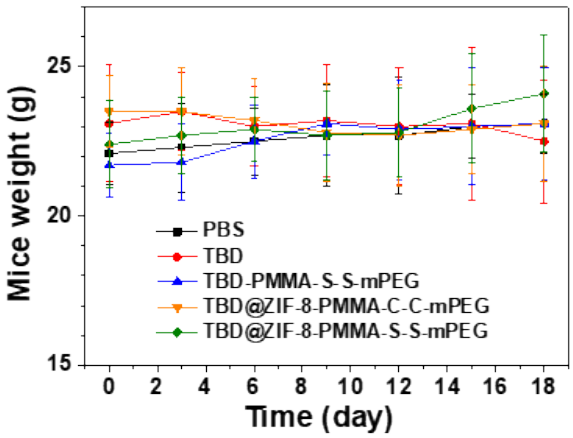


**Figure S32.** Bodyweight changes of mice receiving different treatments, *n* = 5 mice per group.

**References:**

[S1] Wu, W.; Mao, D.; Xu, S.; Ji, S.; Hu, F.; Ding, D.; Kong, D.; Liu, B. High Performance Photosensitizers with Aggregation-Induced Emission for Image-Guided Photodynamic Anticancer Therapy. *Mater. Horiz.* **2017**, *4*, 1110-1114.

[S2] Avci, C.; Imaz, I.; Carné-Sánchez, A.; Pariente, J. A.; Tasios, N.; Pérez-Carvajal, J.; Alonso, M. I.; Blanco, A.; Dijkstra, M.; López, C.; Maspoch, D. Self-Assembly of Polyhedral Metal-Organic Framework Particles into Three-Dimensional Ordered Superstructures. *Nat. Chem.* **2018**, *10*, 78-84.

[S3] Katayama, Y.; Kalaj, M.; Barcus, K. S.; Cohen, S. M. Self-Assembly of Metal-Organic Framework (MOF) Nanoparticle Monolayers and Free-Standing Multilayers. *J. Am. Chem. Soc.* **2019**, *141*, 20000-20003.